Int. J. Electrochem. Sci., 17 **(2022)** Article Number: 221052, doi: 10.20964/2022.10.56

International Journal of
ELECTROCHEMICAL
SCIENCE
www.electrochemsci.org

Corrosion inhibition performance of Cephradine for Q235 steel in acetic acid solutions containing chloride ions

Yongshun Liang[1,2], *Yiyao Li*[3,+], *Haiyang Liu*[1,2], *Minghong Chen*[1,2], *Junming Guo*[1,2], *Mingwu Xiang*[1,2] *and Wei Bai*[1,2,*]

[1] National and Local Joint Engineering Research Center for Green Preparation Technology of Biobased Materials, Yunnan Minzu University, Kunming 650500
[2] Key Laboratory of Green-chemistry Materials in University of Yunnan Province, Yunnan Minzu University, Kunming 650500
[3] School of Chemistry and Chemical Engineering, Shandong University, Jinan 250100
[*]E-mail: bw369852147@qq.com
+ The authors contributed equally to this work as first authors.

Received: 14 July 2022 / *Accepted:* 22 August 2022 / *Published:* 10 September 2022

The corrosion inhibition performance of expired Cephradine for Q235 steel in 20% acetic acid solution containing 600 mg L^{-1} chloride ion has been studied by Tafel polarization curve and electrochemical impedance spectroscopy (EIS). The results show that Cephradine is a good mixed-type inhibitor mainly controlled by cathode, and its adsorption on the Q235 steel surface is in accordance with Langmuir monolayer adsorption. The variation of corrosion inhibition rate with Cephradine concentration, immersion time, and solution temperature was studied. The optimal corrosion inhibition concentration of Cephradine is 1.5×10^{-2} mol L^{-1} at 298 K for 2h, and the inhibition rate reached 86.70%. The inhibition rate reached 96.23% in optimal concentration at 328K for 2h and 96.83% in optimal concentration, 298K for 32h. The scanning electron microscope (SEM), Adsorption model and Electrical conductivity (EC) effectively verified the results.

Keywords: Q235 steel; Acetic acid; Expired drug; Corrosion

1. INTRODUCTION

Q235 low carbon steel is widely used in these fields of construction structure, boiler production, oil/ gas transportation pipeline and machine parts manufacture due to its high strength, good toughness and low cost[1, 2]. Based on the different environment, Q235 steel will be corroded by external substances such as carbon dioxide, water, hydrocarbons, and various organic acids [3, 4], causing severe economic losses and potential safety hazards [5-7]. Therefore, corrosion protection of Q235 steel is very

important, one of the most widely used anticorrosion methods is the addition of organic inhibitors [8-10].

Organic inhibitors usually contain oxygen, nitrogen, sulfur and phosphorous heteroatoms, as well as contain polar functional groups of pi bonds, benzene rings, conjugated double bonds [11]. Thus, it can form a dense and ordered adsorption film on metal surface by physical or chemical adsorption, which can protect metals from corrosive substances [12, 13]. The structure of some drugs is similar to organic corrosion inhibitors. And it is a problem for its disposal after the drug expires. Using expired drugs as corrosion inhibitors can reduce the pollution of expired drugs to the environment, prevent harm to people, realize the recycling of resources, and reduce the economic cost of corrosion inhibitors. Hence, many researchers have conducted a series of studies on the use of expired drugs as corrosion inhibitors in recent years [14-16]. Rana [17] reports the anti-corrosion performance of expired Etoricoxib, the result shows that Etoricoxib is an efficient inhibitor for carbon steel, and the solution temperature has a certain effect on corrosion inhibition performance. Ma [18] studied the corrosion inhibition effect of expired Formoterol in H_2SO_4 media, indicating that Formoterol is a kind of mixed-type corrosion inhibitor with good corrosion inhibition effect. Guo [15] explored the corrosion inhibition performance of three expired Cephalosporins, and found that Ceftriaxone sodium had the best corrosion inhibition performance for carbon steel.

Acetic acid is commonly used in industrial production, chemical cleaning of synthetic fibers and fabrics, metal materials and equipment, and acidified oil recovery technology of oil and gas wells [19, 20], which often causes serious corrosion of equipment during its use [21, 22]. The mechanism of acetic acid corrosion on carbon steel was studied by Sing [23], which indicate that 20% acetic acid solution has the strongest corrosion. And present work shows that 600 mg L^{-1} chloride ion has the highest corrosion rate in acetic acid solution on carbon steel. Therefore, we select Q235 steel as the research object, and uses the expired Cephradine as corrosion inhibitor to investigate the corrosion inhibition behavior of expired Cephradine on Q235 steel in 20% acetic acid solution containing 600 mg L^{-1} chloride ions.

2. MATERIALS AND METHODS

2.1 Materials

All Cephradine capsules are produced by Shanghai Hengshan Pharmaceutical and the structural formula is shown in Fig. 1. Acetic acid was diluted with ultrapure water and added 0.15 g NaCl to make 20% acetic acid solution containing 600 mg L^{-1} chloride ions as corrosion solution (named Cl^-). Q235 steel was produced by Panzhihua Iron and Steel Works, the composition(wt.%) is C 0.07%, Si 0.01%, Mn 0.3%, P 0.022%, S 0.01%, Al 0.03%, Fe remainder.

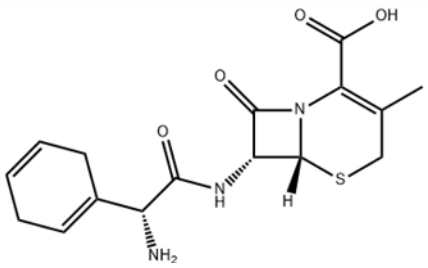

Figure 1. Cefradine structural formula

2.2 Measurement of Tafel polarization curve and electrochemical impedance spectroscopy （EIS）

Electrochemical measurements were tested by the CS350 electrochemical workstation. The electrode with saturated calomel (type 232) and the platinum electrode are used as reference and auxiliary electrodes, respectively. The working electrode was obtained by sealing a 1.0 cm×1.0 cm Q235 steel in a PVC tube with AB glue. The Tafel polarization curves were scanned in the range of ±250 mV (E vs. SCE) at a scan rate of 0.5 mV s^{-1}. EIS was carried out in a frequency range of 100 kHz to 0.01 Hz using a 10 mV peak-to-peak voltage excitation.

The corrosion inhibition rate (η%) was calculated via equations 1 and 2 [24].

$$\eta\% = (\frac{J_{corr}^0 - J_{corr}}{J_{corr}^0}) \times 100\% \qquad 1$$

$$\eta\% = (\frac{R_{ct} - R_{ct}^0}{R_{ct}}) \times 100\% \qquad 2$$

where J_{corr}^0 and R_{ct}^0 stand for the current densities and the charge transfer resistance in Cl^- without the Cephradine. J_{corr} and R_{ct} denote the current densities and the charge transfer resistance in Cl^- with the Cephradine.

Cephradine was dissolved to form different apparent corrosion inhibition concentration. After measuring the concentration (C_{max}) corresponding to the maximum corrosion inhibition rate at 298 K, the working electrode was immersed at 298 K, 303 K, 308 K, 313 K, 318 K, 323 K and 328 K for 2h under C_{max} to investigate the variation of corrosion inhibition rate with temperature; Finally, the working electrode was immersed at 298 K for 2, 4, 8, 16 and 32 hours at C_{max} to investigate the variation of immersion time and corrosion inhibition rate.

2.3 Determination of electrical conductivity

The surface of two pieces of Q235 steel with the specification of 10 mm×10 mm×0.5 mm was polished, cleaned with distilled water 2-3 times, suspended in Cl^- with different concentrations of Cephradine, removed after 6 h of constant temperature for the determination of solution conductivity.

2.4 Morphology analysis

The three parallel samples were soaked in different mediums and temperatures for 6 hours, washed and dried before surface analysis using a scanning electron microscope (SEM, NANOSEM Model 450, FEI, USA, 15 kV).

3. RESULTS AND DISCUSSION

3.1. Tafel polarization curve

As can be seen from Fig. 2, with increase in Cephradine concentration, the corrosion potentials shift negatively, and the slopes of both cathode and anode decrease, particularly cathode, indicating that Cephradine is a mixed-type inhibitor with cathodic predominating [25]. After adding Cephradine, the cathode curves were nearly parallel to each other, indicating that the mechanism of cathode reaction wasn't affected by concentration [26]. Table 1 clearly shows that the current densities gradually decrease with increase in Cephradine concentration, and reach the minimum in 1.5×10^{-2} mol L^{-1}. After the concentration was greater than 1.5×10^{-2} mol L^{-1}, the current densities slightly increased. This means that the highest corrosion inhibition rate (η) was reached at 1.5×10^{-2} mol L^{-1} and the adsorption of Cephradine on the Q235 surface may be reached critical micelle concentration (CMC) in this concentration. The η of each experimental group was calculated by Formula 1. It can be seen the corrosion inhibition efficiency was 86.70% when the Cephradine concentration reached 1.5×10^{-2} mol L^{-1}. The inhibition efficiency values of green corrosion inhibitors reported in the literature are almost in the range of 85% to 95% [17, 26-28]. Fig. 3b and Table 3 show that with increase in immersion time, the cathode and anode slopes and current densities decrease and the η gradually rises. Compared with the expired Acetazolamide [29], the adsorption of Cephradine on the metal surface was greater than desorption with increase in soaking time, and the adsorption film is more uniform and stability, which can better protect the material.

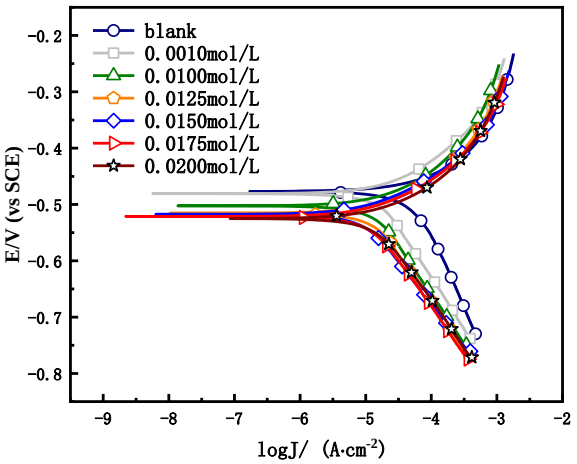

Figure 2. Tafel polarization curve for Q235 steel soaked in Cl^- adding different concentrations of Cephradine for 2 h at 298 K.

Table 1. Polarization parameters for Q235 steel soaked in Cl^- adding different concentration of Cephradine for 2 h at 298 K.

C/ mol·L^{-1}	b_a/ mV·dec^{-1}	b_c/ mV·dec^{-1}	J_{corr}/ μA·cm^{-2}	E/ mV	η/ %
--	131	758	104.57	-477	--
1.0×10^{-3}	104	359	30.355	-409	70.97
1.0×10^{-2}	109	373	27.427	-502	73.77
1.25×10^{-2}	102	339	24.434	-515	76.72
1.5×10^{-2}	84	211	13.906	-517	86.70
1.75×10^{-2}	91	244	17.259	-521	83.50
2.0×10^{-2}	100	254	22.529	-525	78.46

As we can see from Fig. 3a, with increasing temperature, the anode and cathode slopes and current densities increase first and then decrease, indicating that the inhibition rate of Cephradine decreases first and then increases with increase in temperature. If cefradine is adsorbed on Q235 steel only by physical adsorption, the stronger the molecular movement is as the temperature increases, the less cefradine is adsorbed on the Q235 steel, resulting in lower and lower corrosion inhibition, as reported in literature [30]. However, Table 2 showed that the inhibition rate only had a decreasing trend in the range of 298 K to 313 K. Above 313 K, the inhibition rate increases, indicating that the solution absorbs enough energy to cause chemisorption between cefradine and Q235 steel, and creates a more orderly arrangement on the surface of steel sheet [16]. Therefore, the authors concluded that the adsorption mode of Cephradine on Q235 steel under 313 K was primarily based on physical adsorption, and with increase in temperature, the adsorption mode changed from dominant physical adsorption to dominant chemical adsorption.

Table 2. Polarization parameters for Q235 steel soaked in Cl^- at different temperatures for 2 h at C_{max}.

C/ mol·L^{-1}	T/ K	b_a/ mV·dec^{-1}	b_c/ mV·dec^{-1}	J_{corr}/ μA·cm^{-2}	E/ mV	η/ %
1.5×10^{-2}	298	84	211	13.906	-517	86.70
	303	118	243	40.66	-533	61.12
	308	120	273	48.895	-528	53.24
	313	131	246	60.675	-538	41.98
	318	93	193	25.530	-529	75.61
	323	84	137	8.6695	-524	91.71
	328	72	130	3.9415	-515	96.23

Table 3. Polarization parameters for Q235 steel soaked in Cl^- at 298 K for different time at C_{max}.

C/ mol·L^{-1}	t/ h	b_a/ mV·dec^{-1}	b_c/ mV·dec^{-1}	J_{corr}/ μA·cm^{-2}	E/ mV	η/ %
1.5×10^{-2}	2	84	211	13.906	-517	86.70
	4	84	200	11.188	-506	89.30
	8	78	165	7.6948	-506	92.64
	16	77	133	3.9575	-512	96.21
	32	74	132	3.3178	-510	96.83

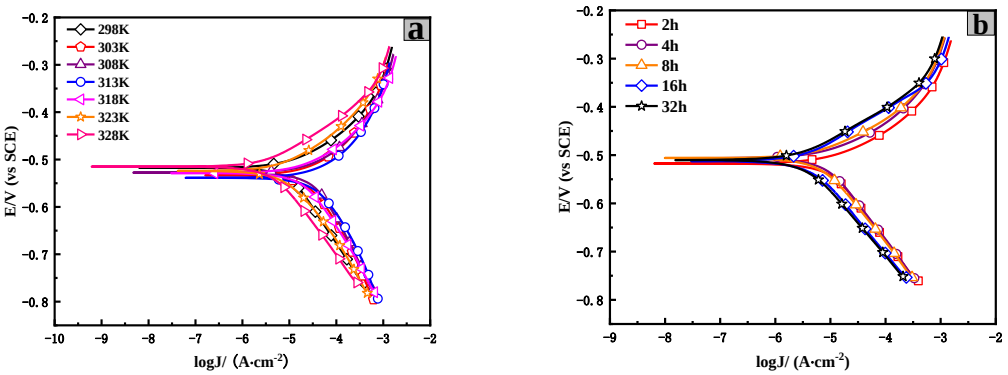

Figure 3. Tafel polarization curve for Q235 steel soaked in Cl^- at C_{max}: (a) different temperatures for 2 h and (b) 298 K for different time.

3.2 Electrochemical impedance spectroscopy (EIS)

In order to match the equivalent circuit diagram more accurately with the actual test circuit in EIS, the author introduces a constant-phase element (CPE) rather than pure double-layer capacitance, so that CPE and R_{ct} are combined in parallel and connected in series with the solution resistance R_s. The equivalent circuit diagram was listed in Fig. 4, and the constant-phase impedance (Z_{CPE}) was calculated by formula 3 [31, 32]:

$$Z_{CPE} = \frac{1}{Q(j\omega)^{\alpha}} \qquad 3$$

Where Q, ω, and j are the magnitude of CPE modulus, angular frequency and imaginary, respectively. The double-layer capacitance (C_{dl})of a circuit containing CPE were obtained by the following formula [32, 33]:

$$C_{dl} = Q(2\pi\omega_{max})^{\alpha-1} \qquad 4$$

$$\omega_{max} = 2\pi f_{max} \qquad 5$$

The f_{max} is the frequency at the maximum value of the imaginary part of the impedance spectroscopy, α represents the deviation parameter (-1≤ α ≤1), usually due to dispersion caused by inhomogeneity and roughness of the solid surface [16]. It is clear from Table 4 that the values of α are all in range of 0.8-1, which verifies that the capacitance formed in the electrochemical system between acetic acid solution and Q235 steel is not an ideal pure capacitance [26]. Moreover, the C_{dl} value in blank

is 176 μF·cm^{-2}, which is greater than other values. Equation 6 was used to explain this phenomenon [34]:

$$C_{dl} = \frac{\varepsilon_0 \varepsilon}{d} S \qquad 6$$

Where ε_0, ε, S and d are the vacuum dielectric constant, local dielectric constant, the bare area of work electrodes, and the thickness of the double-electric layer, respectively. The addition of Cephradine significantly reduced the C_{dl} value, verified the adsorption of Cephradine on the steel surface, reduced the exposed area on the steel surface, and increased the thickness of the double-electric layer. However, the relatively small concentration gradient leads to the heterogeneous distribution of Cephradine sample on the surface of steel plate, whilst resulting in the thickness variation of double electric layer. Therefore, the change of C_{dl} value is irregular.

Fig. 5a shows that after the addition of different concentrations of Cephradine, the Nyquist plot is an irregular semicircle, which indicates that the corrosion of Q235 steel is controlled by the charge transfer process [35]. The irregularity of the semicircle is due to the frequency dispersion caused by the roughness of the electrode surface and adsorption inhomogeneity [36]. The diameter of the semicircle increases with increase in Cephradine concentration and reaches the maximum at 1.5×10^{-2} mol L^{-1}, indicating that the R_{ct} on the surface of Q235 steel reaches the maximum, proving that C_{max} is reached at this time. According to Formula 2, it can be seen the inhibition rate is 75.71% at 1.5×10^{-2} mol L^{-1}.

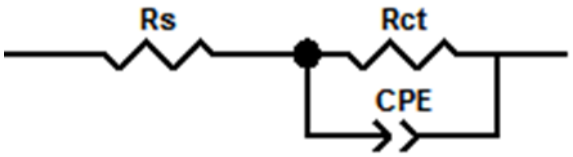

Figure 4. Equivalent circuit diagram of Q235 steel in Cl$^-$.

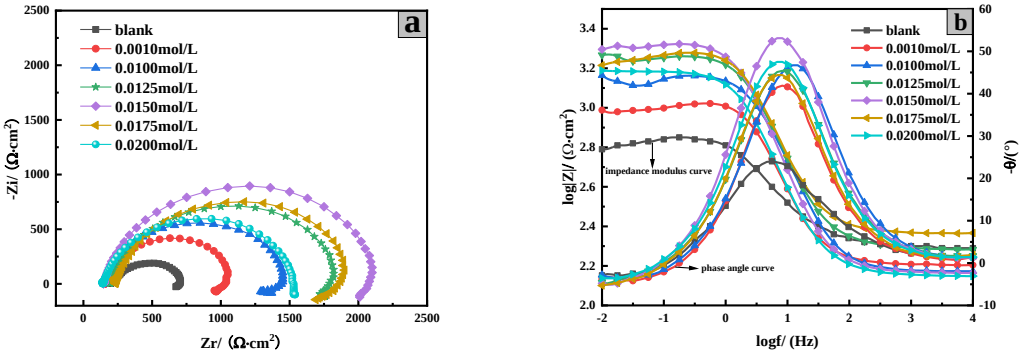

Figure 5. Nyquist plot (a) and Bode diagram (b) of Q235 steel soaked for 2h in Cl$^-$ adding different concentrations of Cephradine at 298 K.

Table 4. Impedance spectrum fitting parameters of Q235 steel immersed in Cl^- adding different concentrations of Cephradine for 2 h at 298 K.

C/ mol·L^{-1}	R_s/ Ω·cm^2	R_{ct}/ Ω·cm^2	C_{dl}/ μF·cm^{-2}	α	η/ %
0	198.2	495.7	176.940	0.79602	—
1.0×10^{-3}	161.8	860	62.664	0.94155	42.36
1.0×10^{-2}	149.4	1269	46.028	0.90109	60.94
1.25×10^{-2}	194.0	1642	52.704	0.88158	69.81
1.5×10^{-2}	147.5	1953	52.040	0.91128	74.62
1.75×10^{-2}	233.6	1620	47.695	0.91041	69.40
2.0×10^{-2}	142.1	1405	74.379	0.88364	64.70

Moreover, it can be seen from the Bode plot (Fig. 5b) that the slopes of impedance modulus plot in the mid-frequency region after adding Cephradine are close to -1, showing typical capacitance characteristics, which verifies the orderly arrangement of Cephradine on Q235 steel [37]. Meanwhile, compared with the blank sample, the impedance modulus values after adding Cephradine are significantly increased, which shows that Cephradine has good corrosion inhibition effect on Q235 steel. The impedance moduli value reaches the maximum when the concentration of Cephradine is 1.5×10^{-2} mol L^{-1}, confirming the corrosion inhibition effect is the best at this concentration. In addition, it can be clearly found a clear peak in the phase angle of the Bode plot, indicating that only one time constant appeared, which was attributed to the relaxation effect caused by the adsorption and desorption of Cephradine molecules on Q235 steel, and verified that the reaction on metal surface was mainly controlled by the charge transfer process [37].

Table 5. Impedance spectrum fitting parameters of Q235 steel soaked in Cl^- at different temperatures for 2 hours at C_{max}.

C/ mol·L^{-1}	T/ K	R_s/ Ω·cm^2	R_{ct}/ Ω·cm^2	C_{dl}/ μF·cm^{-2}	α	η/ %
1.5×10^{-2}	298	147.5	1953	52.040	0.91128	74.62
	303	144.1	1677	67.706	0.89298	70.44
	308	161.4	1193	58.600	0.89108	58.45
	313	151.6	875.3	72.321	0.89421	39.94
	318	156.7	1173	69.116	0.89185	57.74
	323	141.9	1892	62.336	0.89431	73.80
	328	124.2	2603	45.493	0.8754	80.96

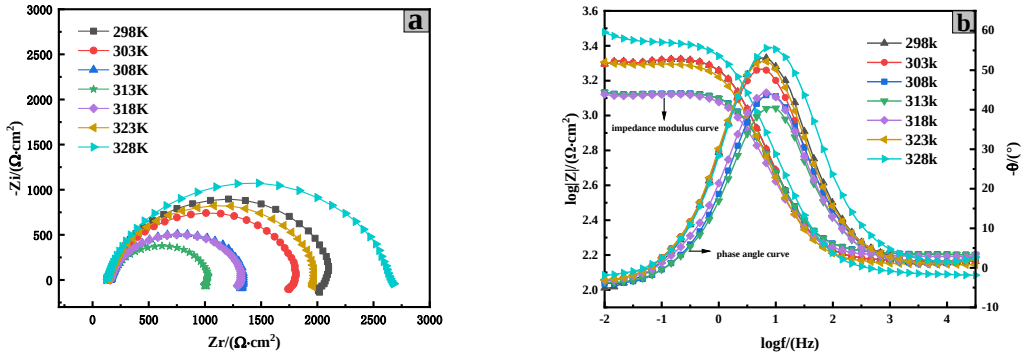

Figure 6. Nyquist plot (a) and Bode diagram (b) of Q235 steel soaked in Cl^- at different temperatures for 2 hours at C_{max}.

It is clear from Fig. 6a that with increasing the temperature, the semicircle goes from big to small, the diameter decreases to the minimum at 313 K, and then gradually increases. Table 5 shows the electrochemical impedance parameters. The results showed that with increase in temperature, both the R_{ct} and η decreased first and then increased. At 313 K, it had the worst corrosion inhibition effect, only 39%. Apparently, Fig 6b shows the same regularity, at low frequencies, the impedance modulus first decreases and then increases with the temperature rise, showing the lowest impedance modulus value at 313 K. The phase angle plot has an extreme value appearing in the mid-frequency region where the impedance module slope is close -1. It indicates that the impedance of the system exhibits a time constant, i.e., the CPE is connected in parallel with R_{ct} and then in series with the solution resistance, sharing a system of synergistic mechanisms [32]. Generally, corrosion inhibition is better when the value of the phase angle is close to 90° [38]. As can be seen from the phase angle figure, with increase in temperature, the phase angle value decreases first and then increases, reaching the minimum at 313 K.

Table 6. Impedance spectrum fitting parameters of Q235 steel soaked in Cl^- for different time at C_{max} and 298K.

C/ mol·L^{-1}	t/ h	R_s/ Ω·cm^2	R_{ct}/ Ω·cm^2	C_{dl}/ μF·cm^{-2}	α	η/ %
1.5×10^{-2}	2	147.5	1953	52.040	0.91128	74.62
	4	202.3	2125	66.79	0.89272	76.67
	8	189.9	2807	48.307	0.90360	82.34
	16	168.7	3157	85.977	0.85885	84.30
	32	184.7	5604	56.321	0.86222	91.14

Fig. 7a shows the radius of the reactance gradually increased with increase in soaking time, indicating that the adsorption amount of Cephradine on the surface of Q235 steel increases gradually with increase in soaking time. It is clear from Table 6, the value of R_{ct} increases and the inhibition rate

gradually increases with increase in soaking time, and the inhibition rate reaches 91.14% for 32 h with increasing the soaking time. Fig. 8 shows the variation laws of EIS and polarization curve is consistent. The η of Cephradine at 298K is similar to that of previously reported expired drugs, but had better inhibitory properties at high temperatures [17, 29, 30, 39-41].

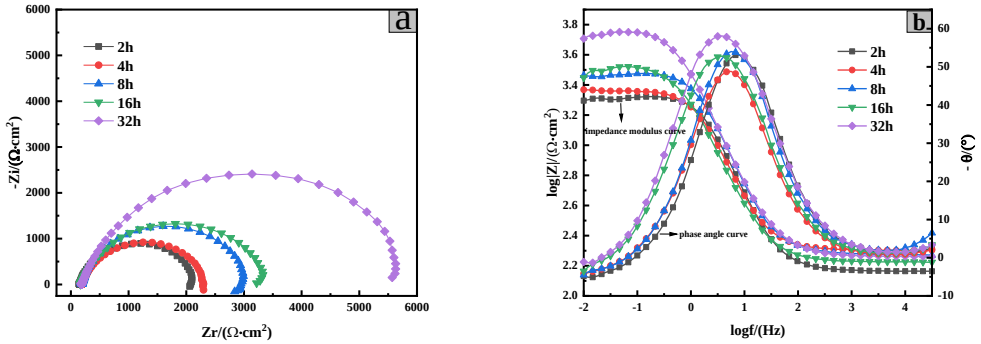

Figure 7. Nyquist plot (a) and Bode diagram (b) of Q235 steel soaked in Cl^- for different time at C_{max} and 298K.

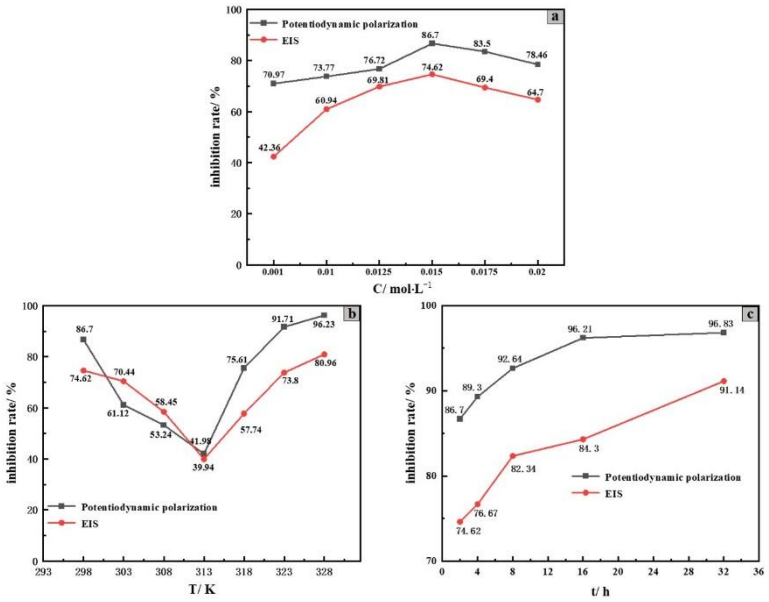

Figure 8. Comparison of Tafel polarization curve and EIS: (a) Concentration - corrosion inhibition rate, (b) Temperature - corrosion inhibition rate, (c) Soaking time - corrosion inhibition rate.

3.3 Adsorption model

In order to further explore the adsorption information of Cephradine molecules on Q235 teel, the authors assume that the adsorption model of Cephradine molecules on Q235 steel conforms to the Langmuir adsorption curve. The adsorption isotherms are as follows [42]:

Langmuir: $\frac{C}{\theta} = \frac{1}{K_{ads}} + C$ 7

Where C, K_{ads}, and θ represent the corrosion inhibitor concentration, adsorption constant, and the surface coverage, respectively. θ was calculated by formula 8 [6, 42]:

$$\theta = \frac{J^0_{corr} - J_{corr}}{J^0_{corr}} \qquad 8$$

It can be seen from Fig. 9a that the Langmuir adsorption curve can well fit with the data, indicating that the adsorption model of Cephradine on Q235 steel surface conforms to the Langmuir adsorption model. The standard free energy of adsorption ΔG^{θ}_{ads} can be calculated by the equation[43]:

$$K_{ads} = \frac{1}{55.1}\exp(-\frac{\Delta G^{\theta}_{ads}}{RT}) \qquad 9$$

Where the K_{ads} is the bonding strength between the adsorbent and the surface, and 55.1 is the molar concentration of water [44]. The value of K_{ads} and ΔG^{θ}_{ads} can be obtained from Table 7. The value of K_{ads} is 1950.5724 L mol^{-1}, which is relatively small, indicating that the adsorption strength between Cephradine and Q235 steel is not very strong at 298 K. Generally, the values of ΔG^{θ}_{ads} up to -20 kJ mol^{-1} are associate with physical adsorption, while those around or more negative than -40 kJ mol^{-1}, represent chemical adsorption [45]. According to the calculation, the value of ΔG^{θ}_{ads} is -28.717 kJ mol^{-1}, indicating that the adsorption of Cephradine molecules on the surface of Q235 steel is a spontaneous adsorption process, and in the case of the adsorption of Cephradine on Q235 steel at 298 K shows up to be a mixed adsorption process dominated by physical adsorption. With increase in temperature, the main adsorption mode of Cephradine will gradually change from physical adsorption to chemical adsorption [46], which verifies the results obtained by Tafel polarization curve and EIS.

Table 7. Parameters related to adsorption curve

Slope	Intercept	R^2	K_{ads}/ L·mol^{-1}	ΔG^{θ}_{ads}/ kJ·mol^{-1}
1.20951	0.00051257	0.98357	1950.5724	-28.717

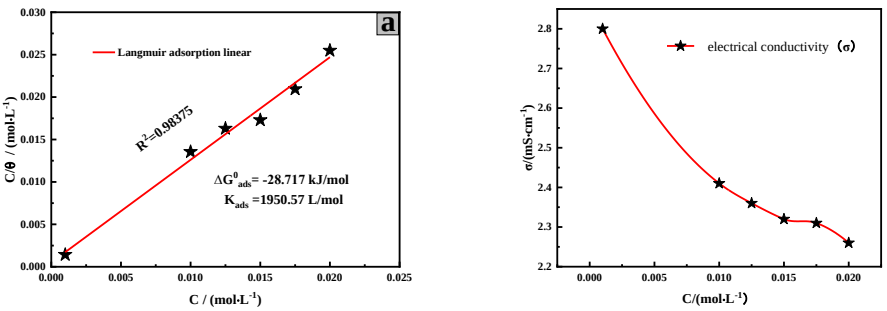

Figure 9. Langmuir adsorption isotherm (a) and concentration-conductivity plots (b) for Q235 steel soaked in Cl^- adding different concentrations of Cephradin at 298 K.

3.4 Determination of electrical conductivity

The polarization and impedance show that the corrosion inhibition rate of Q235 steel reach the maximum when Cephradin concentration increase to 1.5×10^{-2} mol L^{-1}, and the adsorption model is

consistent with monomolecular adsorption. These phenomena suggest that Cephradin might be reached the critical micelle concentration at 1.5×10^{-2} mol L^{-1}. As can be seen from Fig. 9b, with increase in Cephradin concentration, the conductivity of the solution gradually decreases. When the concentration reaches nearby 1.5×10^{-2} mol L^{-1}, the curve inflection point appears, indicating that the critical micelle concentration of Cephradin in the solution has reached [47], which corresponds to the results obtained by the Tafel polarization curve method and EIS. With the further Cephradin concentration increasing, after satisfying monomolecular saturated adsorption and self-micellar formation, the residual cefradine and Ac^- form micellar polymer, which reduces the free HAc with conductivity strength in the solution, leading to a further decrease in conductivity.

Table 8. Conductivity values of Q235 steel immersed in Cl^- adding different concentrations of Cephradine for 6 h at 298 K.

C/（mol/L）	0.0000	0.0010	0.0100	0.0125	0.0150	0.0175	0.0200
σ/（mS·cm^{-1}）	2.85	2.80	2.41	2.36	2.32	2.31	2.26

3.5 Morphology analysis:

Fig. 10 shows the SEM images of Q235 steel immersed in Cl^- under different conditions. Fig. 10a obviously shows that the Q235 steel was severely corroded at 298 K in Cl^- without Cephradin, and forming corrosion pits of different sizes. In the presence of Cephradin (Fig. 10b), the damage of Q235 steel is obviously reduced, the surface is smooth and flat, just a few very small corrosion holes, and even can see the traces of steel treatment before immersion, indicating that Cephradin has a good corrosion inhibition effect for Q235 steel in Cl^- at 298 K. As can be seen from Fig. 10c, at 323 K, with the adding Cephradin in Cl^-, the surface of Q235 steel shows no signs of corrosion, but also can't see the traces of processing. This is because at the temperature of 323 K, Cephradin form a more tightly bound adsorption layer on Q235 steel, mainly by chemisorption. This adsorption layer can be observed with the naked eye and still exists even after ultrasonic cleaning, suggesting that the adsorption layer is very tight and more precise for protecting Q235 steel. The SEM measurement results well validate the results of Tafel polarization curve and EIS.

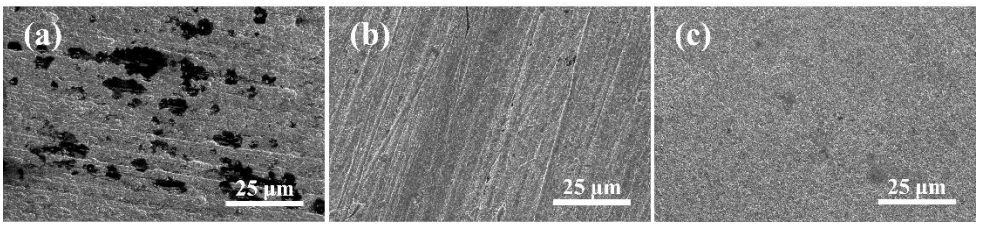

Figure 10. SEM figure of Q235 steel soaked in Cl^-: (a) without Cephradin at 298 K, (b) adding 1.5×10^{-2} mol/ L Cephradin at 298 K, (c) adding 1.5×10^{-2} mol/ L Cephradin at 323 K.

3.6 Corrosion inhibition mechanism:

The corrosion inhibition mechanism is shown in Fig. 11. Cephradin contains strong polar groups such as carboxyl, hydroxyl and heterocyclic compound containing N and S atoms. These groups will replace the original Cl^-, Ac^-, H_2O and other particles adsorbed on the surface Q235 steel, forming a thicker adsorption layer that prevents particles in solution from coming into contact with and reacting with iron, thus inhibiting its dissolution of anode. Moreover, Cephradin contains amino, which is easily protonated and positively charged in the acidic environment. The protonated amino directly competes with the hydrogen ions in acetic acid and adsorbs in the corrosion cathode area to inhibit the occurrence of cathode hydrogen evolution reaction.

As the temperature rises, the internal energy of solution system will increase, leading to the acceleration of the movement of molecules in the solution. By this time, the adsorption energy of Cephradin cannot offset the kinetic energy. Therefore, Cephradin could not form a stable adsorption film on the surface of steel, which aggravated the corrosion of acetic acid solution on Q235 steel. When the temperature rises to a certain value, the solution absorbs enough energy to pass through the reaction energy barrier, Cephradin reacts chemically with Q235 steel, and the adsorption mechanism changes from mainly physical adsorption to mainly chemical adsorption. At this point, Cephradin chemically bonds to the surface of the steel sheet, the kinetic energy of Cephradin cannot offset the chemical adsorption energy, making the protective film generated on Q235 steel more solid, resulting in an increase of the corrosion inhibition rate.

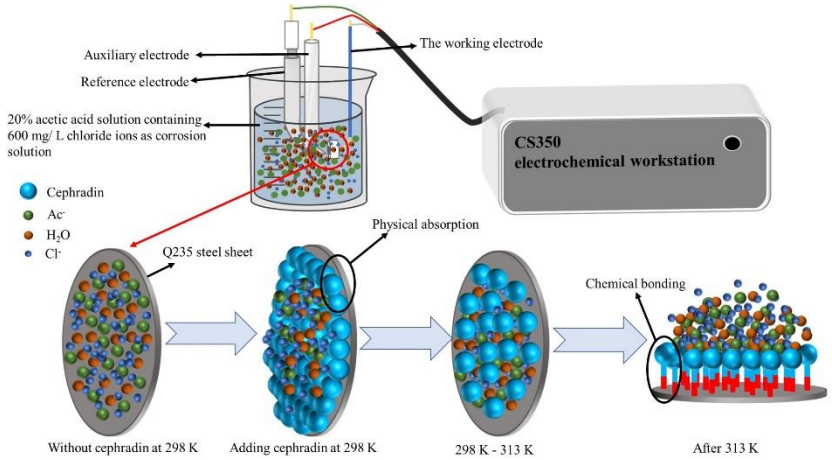

Figure 11. Corrosion inhibition mechanism of cephradin

4. CONCLUSION

The results show that Cephradine is a good mixed-type inhibitor mainly controlled by cathode, and its adsorption on Q235 steel surface is consistent with Langmuir monolayer adsorption. With increase in Cephradin concentration, the corrosion inhibition rate was the first to increase and then to decrease, reaching the maximum corrosion inhibition rate of 86.70% at 1.5×10^{-2} mol L^{-1}, and the

adsorption of Cephradin on Q235 steel is mainly by physical adsorption at 298 K. With soaking time growth, the η gradually became larger and reached 96.83% at 32 h. With temperature increasing, η is the first to decrease, at 313 K is the smallest, and then gradually become larger, to 323 K corrosion inhibition rate more than 90% and 96.23% at 328K. The adsorption mode gradually changes from mainly physical to mainly chemical adsorption.

CONFLICTS OF INTEREST
There are no conflicts to declare.

ACKNOWLEDGEMENTS
This work financial support from the Yunnan Fundamental Research Projects Youth Fund (No. 202001AU070008) and the National Natural Science Foundation of China (No. 51972282 and U1602273).

References

1. S.J. Chen, S.Y. Chen, B. Zhu, C.B. Huang and W.P. Li, *J. Mol. Liq.,* 311 (2020) 113312.
2. M. Finšgar and J. Jackson, *Corros. Sci.,* 86 (2014) 17-41.
3. K. Suzumura and S. Nakamura, *J. Mater. Civ. Eng.,* 16 (2004) 1-7.
4. L.L. Liao, S. Mo, H.Q. Luo and N.B. Li, *J. Colloid Interface Sci.,* 520 (2018) 41-49.
5. C. Verma, K.Y. Rhee, M.A. Quraishi and E.E. Ebenso, *J. Taiwan Inst. Chem. Eng.,* 117 (2020) 265-277.
6. A.M. Eldesoky, H.M. Hassan, A. Subaihi, A.E. Shahawy and T.A. Farghaly, *Coatings,* 10 (2020) 167.
7. B.R. Hou, X.G. Li, X.M. Ma, C.W. Du, D.W. Zhang, M. Zheng, W.C. Xu, D.Z. Lu and F.B. Ma, *npj Mater. Degrad.,* 1 (2017) 4.
8. S. Sharma and A. Kumar, *J. Mol. Liq.,* 322 (2021) 114862.
9. T.J. Harvey, F.C. Walsh and A.H. Nahlé, *J. Mol. Liq.,* 266 (2018) 160-175.
10. G. Cui, Z.X. Bia, S.H. Wang, J.G. Liua, X. Xing, Z.L. Li and B.Y. Wang, *Prog. Org. Coat.,* 148 (2020) 105821.
11. Y.J. Qiang, S.L. Fu, S.T. Zhang, S.J. Chen and X.F. Zou, *Corros. Sci.,* 140 (2018) 111-121.
12. C. Verma, E.E. Ebenso, I. Bahadur and M.A. Quraishi, *J. Mol. Liq.,* 266 (2018) 577-590.
13. L. Guo, J.H. Tan, S. Kaya, S.L. Leng, Q.B. Li and F. Zhang, *J. Colloid Interface Sci.,* 570 (2020) 116-124.
14. G. Gece, *Corros. Sci.,* 53 (2011) 3873-3893.
15. W.J. Guo, A. Umar, Q. Zhao, M.A. Alsaiari, Y. Al-Hadeethi, L.Y. Wang and M.S. Pei, *J. Mol. Liq.,* 320 (2020) 114295.
16. H.M. Elabbasy and H.S. Gadow, *J. Mol. Liq.,* 321 (2020) 114918.
17. R.A. Anaee, I.H.R. Tomi, M.H. Abdulmajeed, S.A. Naser and M.M. Kathem, *J. Mol. Liq.,* 279 (2019) 594-602.
18. X.R. Ma, R. Dang, Y.H. Kang, Y. Gong, J. Luo, Y.Y. Zhang, J.W. Fu, C.Y. Li and Y.J. Ma, *Int. J. Electrochem. Sci.,* 15 (2020) 1964-1981.
19. M. Lagrenée, B. Mernari, M. Bouanis, M. Traisnel and F. Bentiss, *Corros. Sci.,* 44 (2002) 573-588.
20. Y. Wu, Y.L. Shi, C.W. Su, L.L. Feng, J.M. Guo and W. Bai, *Int. J. Electrochem. Sci.,* 12 (2017) 10042-10056.
21. J. Amri, E. Gulbrandsen and R.P. Nogueira, *Electrochem. Commun.,* 10 (2008) 200-203.
22. A.Y. Adesina, I.B. Obot, A.A. Sorour, S. Mtongana, S.B. Mamilla and A.A. Almathami, *Eng.*

Failure Anal., 127 (2021) 105511.
23. M.M. Singh and A. Gupta, *CORROSION,* 56 (2000) 371-379.
24. H. Gerengi, M. Mielniczek, G. Gece and M.M. Solomon, *Ind. Eng. Chem. Res.,* 55 (2016) 9614-9624.
25. W.W. Zhang, B. Nie, M.F. Wang, S.H. Shi, L. Gong, W.J. Gong, H. Pang, X.W. Liu, B.Z. Li, Y.Y. Feng and Y.C. Wu, *J. Mol. Liq.,* 343 (2021) 117672.
26. H. Li, Y.J. Qiang, W.J. Zhao and S.T. Zhang, *Colloids Surf., A,* 616 (2021) 126077.
27. E. Alibakhshi, M. Ramezanzadeh, G. Bahlakeh, B. Ramezanzadeh, M. Mahdavian and M. Motamedi, *J. Mol. Liq.,* 255 (2018) 185-198.
28. L.Y.S. Helen, A.A. Rahim, B. Saad, M.I. Saleh and P.B. Raja, *Int. J. Electrochem. Sci.,* 9 (2014) 830-846.
29. L.P. Chaudhari and S.N. Patel, *J. Bio- Tribo-Corros.,* 5 (2019) 20.
30. A.S. Fouda, M.A.E. Morsi and T.E. Mogy, *Green Chem. Lett. Rev.,* 10 (2017) 336-345
31. J. Haquea, V. Srivastavaa, M.A. Quraishib, D.S. Chauhanb, H. Lgazc and I.M. Chungc, *Corros. Sci.,* 172 (2020) 108665.
32. Y. Qiang, S. Zhang and L. Wang, *Appl. Surf. Sci.,* 492 (2019) 228-238.
33. M.A. Hegazy, M. Abdallah, M.K. Awad and M. Rezk, *Corros. Sci.,* 81 (2014) 54-64.
34. B.C. Tan, S.T. Zhang, W.P. Li, X.L. Zuo, Y.J. Qiang, L.H. Xu, J.Y. Hao and S.J. Chen, *J. Ind. Eng. Chem.,* 77 (2019) 449-460.
35. L. Larabi, Y. Harek, M. Traisnel and A. Mansri, *J. Appl. Electrochem.,* 34 (2004) 833-839.
36. L.O. Olasunkanmi and E.E. Ebenso, *J. Colloid Interface Sci.,* 561 (2020) 104-116.
37. Y.J. Qiang, L. Guo, H. Lia and X.J. Lana, *Chem. Eng. J.,* 406 (2021) 126863.
38. A. Singh, K.R. Ansari, J. Haque, P. Dohare, H. Lgaz, R. Salghi and M.A. Quraishi, *J. Taiwan Inst. Chem. Eng.,* 82 (2018) 233-251.
39. A.S. Fouda, W.M. Mahmoud and H.A.A. Mageed, *J. Bio- Tribo-Corros.,* 2 (2016) 7.
40. P. Geethamani and P.K. Kasthuri, *J. Taiwan Inst. Chem. Eng.,* 63 (2016) 490-499.
41. R.G. Sundaram, G. Vengatesh, M. Thamaraiselvi, R. Prabakaran, V. Thailan, I. Muthuvel and S. Niraimathi, *J. Iran. Chem. Soc.,* 19 (2022) 2311-2329.
42. L. Guo, R.L. Zhang, B.C. Tan, W.P. Li, H.Y. Liu and S.Z. Wu, *J. Mol. Liq.,* 310 (2020) 113239.
43. B. Xu, W.Z. Yang, Y. Liu, X.S. Yin, W.N. Gong and Y.Z. Chen, *Corros. Sci.,* 78 (2014) 260-268.
44. Z.W. Wang, W. Bai, Y. Yang, Y. Wu, C.W. Su and J.M. Guo, *Int. J. Electrochem. Sci.,* 11 (2016) 6110-6125.
45. A. Kosari, M.H. Moayed, A. Davoodi, R. Parvizi, M. Momen, H. Eshghi and H. Moradi, *Corros. Sci.,* 78 (2014) 138-150.
46. M.M. Solomon, H. Gerengi and S.A. Umoren, *ACS Appl. Mater. Interfaces,* 9 (2017) 6376–6389.
47. C. Th´evenot, B. Grassl, G. Bastiat and W. Binana, *Colloids Surf., A,* 252 (2005) 105-111